Use of a Phase Reference for Field Mapping with Amplitude Images at Low Field

D. Tomasi, [1,2] H. Panepucci, [3] E. L. Vidoto, [4] and E. Ribeiro Azevedo [5]

Instituto de Física da Universidade de São Paulo, São Carlos, Brazil

We present a method to obtain MRI amplitude images that can picture the magnetic field due to arbitrary shaped magnetized objects. The method employees the gradient recalled echo sequence and two sets of data obtained in separate experiments, one of which provides a phase reference image making it possible to eliminate the effect of the B_0 field inhomogeneities. The final magnitude images have a good signal-to-noise even at low fields, and provide qualitative as well as quantitative information about the magnetic field produced by the ferromagnetic object. As an example the method is applied to study the field produced by a small metal piece in a 500-G scanner, and the experimental results are compared with numerical simulations.   © 1998 Academic Press

INTRODUCTION

In the past few years several studies using high strength field magnets have been performed in order to understand the artifacts observed in MR images due to the presence of objects exhibiting magnetic (*1–3*) or metallic (*5, 6*) properties.

The susceptibility artifacts induced in images performed with spin-echo (SE) sequences are caused by large and abrupt changes in magnetic susceptibilities and appear particularly pronounced when using low readout gradients (*1*). For gradient-echo (GRE) sequences the artifacts are due to the loss of spin coherence inside each voxel. This takes place during the evolution time (*2, 3*) and is due to the susceptibilities induced and the static field inhomogeneities.

Artifacts induced by metallic implants are well recognized on MR images (*7*). These are highly dependent on metal type and are less quantitatively studied than the susceptibility artifacts. Small quantities of iron (0.01–1.7 mg.) (*6*) cause circular or elliptic-shaped black areas in GRE or SE se-

quences, respectively. The artifact size increases with the amount of ferromagnetic material but no dependence on the magnetic field strengths was observed (*6*). For metals with very low susceptibility, such as diamagnetic cooper ($\chi \sim -2 \times 10^{-5}$), the eddy currents are the dominant effect, whereas for weakly paramagnetic metals with a slightly larger susceptibility, such as titanium ($\chi \sim 2 \times 10^{-5}$), both susceptibility and eddy currents artifacts can be observed (*5*).

In this paper we analyze the artifacts induced by weakly ferromagnetic metals ($\chi \sim 2 \times 10^{-1}$) in GRE sequences. Here we show that the dephasing effects could be put in evidence more clearly by a special subtraction procedure.

THEORY

The susceptibility artifacts have been explained previously considering the effects of intravoxel dephasing on the time domain signals (*3*). In this paper we concentrate on the amplitude-image artifacts due to weak ferromagnetic metals.

In a GRE experiment the spins are partially refocused at echo-time due to the reversed readout gradient. In the rotating frame the spins at (x, y, z) precess with an extra offset frequency that depends on the z component of the B_0 magnetic field inhomogeneity at that position, $\delta B(x, y, z)$. Therefore at the echo time t_0, the spins accumulate a phase

$$\phi(x, y, z) = \gamma \delta B(x, y, z) t_0, \qquad [1]$$

where γ is the proton–gyromagnetic ratio. For a slice in the (x, z) coronal plane, the k-space signal coming from the excited spins in the sample can be written as

$$S_0(k_x, k_z) = \int m(x, y, z) \exp\{i\phi(x, y, z)\}$$
$$\times \exp\{i(k_x x + k_z z)\} d^3 r, \qquad [2]$$

[1] On leave from the Escuela de Ciencia y Tecnologia, Universidad Nacional de San Martin, Alem 3901, 1651 San Andres, Buenos Aires, Argentina.
[2] E-mail: tomasi@ifqsc.sc.usp.br.
[3] E-mail: pane@ifqsc.sc.usp.br.
[4] E-mail: vidoto@ifqsc.sc.usp.br.
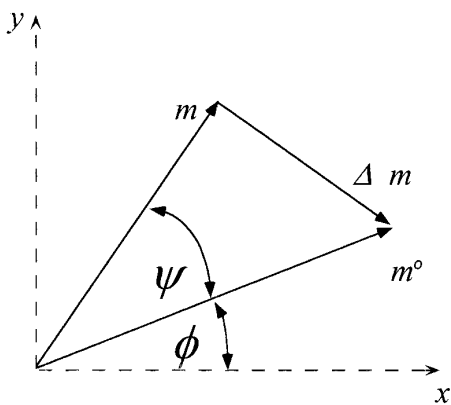[5] E-mail: azevedo@ifqsc.sc.usp.br.

$$k_i = \gamma \int_0^{t_0} G_i(\tau) d\tau. \qquad [3]$$

In the presence of a weak ferromagnetic object the extra magnetic field inhomogeneity $\Delta B_z(x, y, z)$ introduces an additional spin phase shift $\psi(x, y, z) = \gamma \Delta B_z(x, y, z) t_0$. The signal resulting from the excited spins in the whole sample reflects the magnetization evolution under both fields $\delta B(x, y, z)$ and $\Delta B_z(x, y, z)$

$$S(k_x, k_z) = \int m(x, y, z)$$
$$\times \exp\{i[\phi(x, y, z) + \psi(x, y, z)]\}$$
$$\times \exp\{i(k_x x + k_z z)\} d^3 r. \qquad [4]$$

Due to the discreetness of the acquisition process the intensity of the pixel associated with a given voxel at position r will correspond to the magnetization average over the voxel volume V, $\mathbf{m}$, given by

FIG. 1. Vector diagram showing the principle of the proposed method. m^o and m represent the amplitude and phase of the voxel magnetization before and after introducing the magnetic object. The difference in size represents the effect of intravoxel dephasing while ψ measures the additional phase due to the extra field ΔB_z. Notice that even if $|m^o| - |m|$ might be small, $|\Delta m|$ is strongly dependent on ψ, i.e., ΔB_z.

where k_z and k_x are related to the readout and phase encoding gradients (G_z, G_x), respectively, by
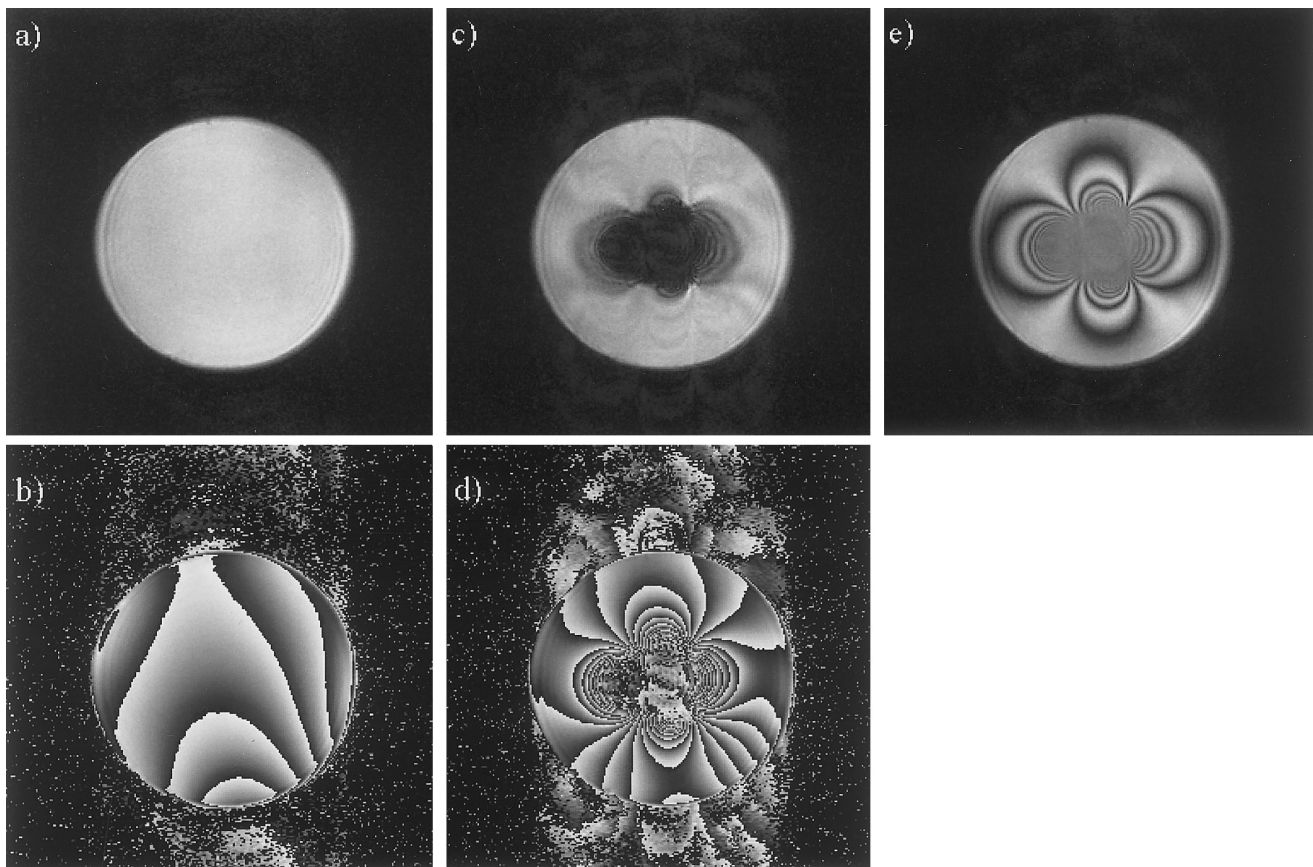

FIG. 2. GRE amplitude images of the 2 mM $CuSO_4$ phantom. (a) Reference image of the phantom reconstructed from the S_0 data set; (c) image of the phantom with the ferromagnetic object reconstructed from the S data set; (e) amplitude image reconstructed from the difference between the two data sets; (b and d) are the phase images reconstructed from the S_0 and S data sets, respectively. Slice thickness = 1 cm, TE = 25 ms, TR = 500 ms.
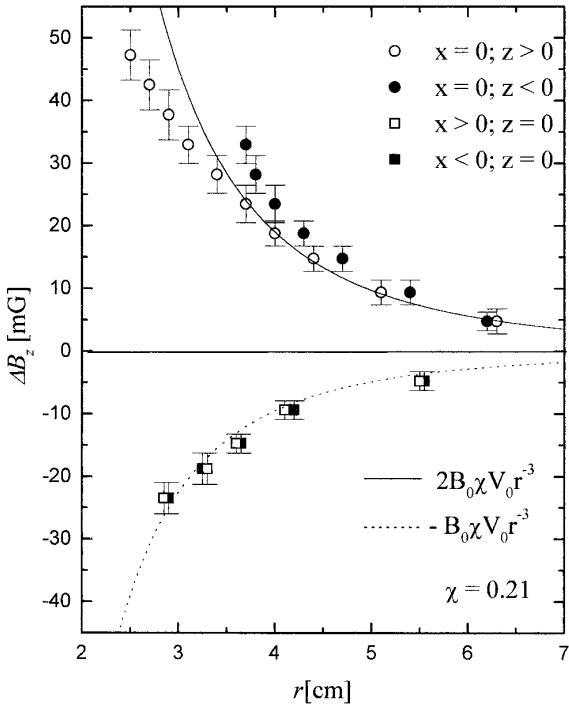
FIG. 3. Plot of the magnetic field due to the magnetic object obtained from the image in Fig. 2e. The solid and open circles correspond to the observed dependence along the $z < 0$ and $z > 0$ axes, respectively. Solid and open squares are the same for the $x < 0$ and $x > 0$ axes, respectively. The solid and dashed lines show r^{-3} dependence expected for the dipole field (see Eq. [9]).

$$\mathbf{m} = \int_V m(\xi, \eta, \zeta)$$
$$\times \exp\{i[\phi(\xi, \eta, \zeta) + \psi(\xi, \eta, \zeta)]\}\, d\xi d\eta d\zeta. \quad [5]$$

In regions where the field varies rapidly, $|\mathbf{m}|$ goes to zero, leading to the well-known signal void in the image. Where the field varies more slowly the phase of $\mathbf{m}$ contains the information about the average local field which involves the static field inhomogeneity contribution ϕ and the ferromagnetic object contribution ψ that is being sought.

To get a map of the magnetic field, ΔB_z, produced by the ferromagnetic object we must known ψ. This could be accomplished by a two-measurement experiment using a uniform phantom with and without the ferromagnetic object by subtraction of the phase images.

Due to the unavoidable presence of intrinsic inhomogeneities in the B_0 field, this procedure has a serious draw back. In fact from Eq. [1] it would seem desirable to use long echo times t_0, to get better resolution in the field maps. The combination of long echo times and or large B_0 field inhomogeneities may cause ϕ in Eq. [1] to become larger than π, making it a nonmonotonic function of position seriously hindering the subtraction process. This is further

worsened by the intrinsic noise characteristic of phase images, specially at low fields.

On the other hand it is possible to extract the relevant phase information from a magnitude image by using the $S_0(k_x, k_z)$ data as a phase reference, that is, by calculation of an amplitude image reconstructed from the difference set $\Delta S = S - S_0$. From Eq. [2] and Eq. [4] one has

$$\Delta S(k_x, k_z) = \int m(x, y, z)$$
$$\times (\exp\{i[\phi(x, y, z) + \psi(x, y, z)]\}$$
$$- \exp\{i\phi(x, y, z)\})$$
$$\times \exp\{i(k_x x + k_z z)\}\, d^3r. \quad [6]$$

The complex Fourier transform of Eq. [6] gives the quantity

$$m(x, z)\exp\{i\phi(x, z)\}(\exp\{i\psi(x, z)\} - 1)$$
$$= \Delta \mathbf{m}(x, z), \quad [7]$$

which can be viewed as the difference between two transverse magnetization vectors whose phases result from the evolution in the presence only of the B_0 inhomogeneity or the total field, including the effects of the ferromagnetic object. Figure 1 shows this situation in a graphical way.

The modulus of this complex Fourier transform

$$\Delta m(x, z) = m(x, z)|1 - \exp\{i\psi(x, z)\}| \quad [8]$$

gives an image where the intensity is modulated by ψ, which is proportional to the z component of the magnetic field due to the ferromagnetic object. If a uniform phantom is used, this gives a map of that field.

This procedure removes the effects of the DC field inhomogeneity and results in a good signal-to-noise image that pictures the constant field contours due to the ferromagnetic object.

EXPERIMENTAL RESULTS

To test the above method we used a simple uniform phantom consisting of a 20-cm diameter cylindrical container filled with 2 mM $CuSO_4$ water solution.

A GRE sequence with TE = 25 ms and TR 500 ms was used to image the phantom in our 0.05-T home-made system that uses a resistive full-body Hitachi magnet which has a B_0 field homogeneity of 50 ppm in a 30-cm spherical diameter volume. One-centimeter-thick coronal images having 1 mm in plane resolution were obtained using 0.345 and 0.075 G/cm slice selection and readout gradients, respectively.

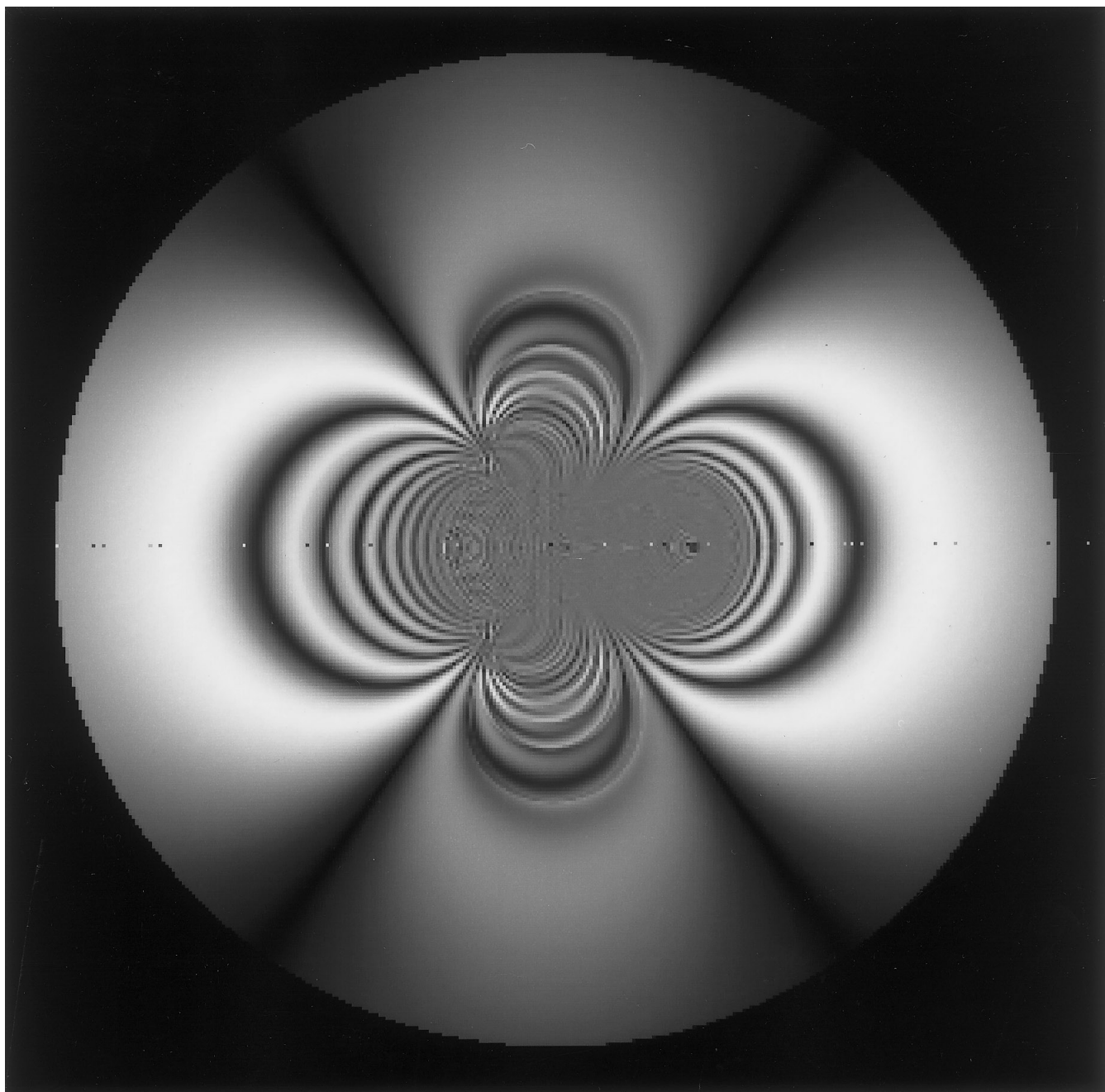Two sets of image data S_0 and S were acquired before

FIG. 4. Numerical simulation of the phase difference image.

and after placing a 43-mg piece of 304 stainless steel at the center of the phantom, respectively.

Figures 2a and 2c show the amplitude images corresponding to the S_0 and S data sets, respectively. Although Fig. 2c shows the effect of the ferromagnetic object that results in signal loss and geometrical distortion plus a complex band pattern, it does not reveal clearly the magnetic field pattern expected from a small dipole.

Figure 2e shows the amplitude image obtained from the

Fourier transform of the difference set $S - S_0$ that according to Eq. [8] measures Δm and reveals purely the field changes introduced by the magnetic inclusion.

Although geometrical distortion and some signal loss are still present near the ferromagnetic object, the interference pattern resulting from the difference in magnetic field distribution in the two experiments clearly shows the shape of the equal field contours expected from a dipole point.

To show how the presence of static field inhomogeneities

precluded the direct use of phase images to map the field of the magnetic object, we show in Figs. 2b and 2d the phase images obtained from the two separate data sets, S_0 and S, which clearly illustrate the problem discussed earlier in text.

The actual values of this field ΔB_z can be obtained for the points where $\psi = 2n\pi$ or $(2n + 1)\pi$ which are the minimum and maximum image intensities. The values of ΔB_z thus obtained from Fig. 2e are plotted in Fig. 3 as a function of the distance r from the ferromagnetic object along the x and z axes. Two sets of points are plotted, corresponding to whether ΔB_z is parallel or antiparallel to the encoding gradient fields. It can be noticed that due to the geometrical distortion effect (1) the two sets are different along the readout z direction but are coincident to within two pixels along the phase encoding x direction. From the fitting of the experimental points along the x direction, show as a dotted line in Fig. 3, a value of $\chi = 0.21 \pm 0.01$ was obtained. The solid line in Fig. 3 is the expected field along z calculated using the above susceptibility value, using

$$\Delta B_z(x, y, z) = -B_0 \chi V_o \frac{2z^2 - x^2 - y^2}{(x^2 + y^2 + z^2)^{5/2}}, \quad [9]$$

where V_o is the ferromagnetic object volume.

Numerical simulations were made for calculating both the GRE images and those obtained by the above subtraction procedure. In the simulations the effects of geometrical distortion were included according to Ref. (1).

The magnitude and phase of the transverse magnetization for each voxel were calculated according to Eq. [5]. To perform the integration over the voxel volume a variable grid of N^2 elements was employed where N was chosen according to the intensity of the dipole field at the voxel location.

The images were plotted as the modulus of the calculated magnetization m. The results of this simulation are shown in Fig. 4, which must be compared with the experimental results shown in Fig. 2e.

CONCLUSION

Although the presence of magnetic objects provokes artifacts in the MRI images regardless of the method employed for imaging, the artifacts produced in GRE sequences can in principle give a map of the magnetic field due to the ferromagnetic object from which the magnetic susceptibility χ could be extracted. Usual amplitude GRE images contain this information but, due to the signal void in the proximity of the region of χ discontinuity, detailed information on the field distribution in those regions is difficult to obtain. Furthermore the intensity modulation observed in GRE images result from the intravoxel dephasing and are therefore strongly dependent on voxel size. Phase images can solve some of this problems but are inherently noisy, particularly at low field, thus preventing the use of low field scanners for studying the susceptibility or field distribution even for weakly ferromagnetic objects.

The use of a phase reference overcomes this problems, resulting in good signal-to-noise images that actually show clearly the contours of magnetic field intensity and could be used to map the field produced by arbitrary-shaped objects which could be difficult to calculate.

REFERENCES

1. K. M. Lüdeke, P. Röschmann, and R. Tischler, *Magn. Reson. Imaging* **3**, 329 (1985).

2. Z. H. Cho and Y. M. Ro, *Magn. Reson. Med.* **23**, 193 (1992).

3. C. J. G. Bakker, R. Bhagwandien, M. A. Moerland, and M. Fuderer, *Magn. Reson. Imaging* **11**, 539 (1993).

4. M. A. Brown, J. A. Carden, R. E. Coleman, R. McKinney, and L. D. Spicer, *Magn. Reson. Imaging* **5**, 443 (1987).

5. L. H. Bennett, P. S. Wang, and M. J. Donahue, *J. Appl. Phys.* **79**, 4712 (1996).

6. A. Alanen, S. Bondestem, and M. Komu, *Acta Radiol.* **36**, 92 (1995).

7. F. G. Shellock and J. S. Curtis, *Radiology* **180**, 541 (1991).